

# Development of CISPH method for accurate water-surface tracking in breaking waves

A. Khayyer <sup>a</sup>, H. Gotoh <sup>b,\*</sup>, S. D. Shao <sup>c</sup>

<sup>a,b</sup> *Department of Urban and Environmental Engineering, Kyoto University, Katsura Campus, Nishikyo-ku, Kyoto 615-8540, Japan*

<sup>c</sup> *School of Engineering, Design and Technology, University of Bradford, West Yorkshire, BD7 1DP, United Kingdom*

## Abstract

A Corrected Incompressible SPH (CISPH) method is proposed for accurate tracking of water surface in breaking waves. Corrective terms are derived based on a variational approach to ensure the angular momentum preservation of Incompressible SPH (ISPH) formulations. The proposed CISPH model is applied to solve the Navier-Stokes equation for simulating the breaking and post-breaking of solitary waves on a plane slope. The high precision of the CISPH model is confirmed through both qualitative and quantitative comparisons with experimental data. The introduction of corrective terms significantly improves the capability and the accuracy of the ISPH model in the simulation of wave breaking and post-breaking.

*Keywords:* CISPH model, ISPH model, SPH method, particle method, wave breaking, angular momentum preservation properties

## 1. Introduction

Tracking the movement of interface boundaries such as the free surfaces is of crucial importance in many numerical hydrodynamic calculations. Despite the recent advances in the introduction of high-order grid-based water-surface-tracking techniques, still there are difficulties to accurately analyze problems in which the free surface undergoes abrupt and large deformations (such as the case of breaking waves) and especially when fragmentation and coalescence of water exist (such as the process of splash up in the post-breaking stage).

---

\* Corresponding Author TEL: +81-75-383-3310 FAX: +81-75-383-3311  
Email: [gotoh@mbox.kudpc.kyoto-u.ac.jp](mailto:gotoh@mbox.kudpc.kyoto-u.ac.jp)

Recently, Particle Methods which are among the meshfree or gridless methods have been used in many engineering applications as well as the simulation of hydrodynamic flows. In the Particle Methods, the state of a system is represented by a set of discrete particles, without a fixed connectivity, followed in a Lagrangian manner. Hence, moving interfaces and free surfaces can be more easily analyzed and tracked by the Particle Methods than by the conventional grid-based methods. Moreover, fully Lagrangian treatment of particles, allows the convection terms to be calculated without numerical diffusion which is an inherent problem in grid-based calculations.

As one of the earliest Particle Methods, the Smoothed Particle Hydrodynamics (SPH) method was proposed for astrophysical applications (Lucy, 1977; Gingold and Monaghan, 1977) but has since been extended to model a wide range of engineering applications including elasticity (Libersky and Petschek, 1991), multiphase-flows (Monaghan and Kocharyan, 1995) and blood simulation for virtual surgery (Muller *et al.*, 2004). The SPH method has also been extended and applied to simulate the incompressible flows by treating the flow as slightly (or weakly) compressible with an appropriate equation of state (Monaghan, 1994; Morris *et al.*, 1997). The Weakly Compressible SPH (WCSPH) model has been utilized for many applications such as runup and rundown of waves on beaches (Monaghan and Kos, 1999), wave breaking on arbitrary structures (Colagrossi and Landrini, 2003; Monaghan *et al.*, 2004) and wave breaking and post-breaking on beaches (Dalrymple and Rogers, 2005).

An alternative and favored approach to enforce the incompressibility in the SPH method is to apply a two-step projection method similar to that in the Moving Particle Semi-Implicit (MPS) method (Koshizuka and Oka, 1996). Based on this approach, Cummins and Rudman (1999) proposed an Incompressible SPH (ISPH) method in which an intermediate velocity field is projected onto a divergence free space by solving a Pressure Poisson Equation derived from an approximate projection. Analogous to this SPH projection method, Shao and Lo (2003) developed a strictly ISPH method for the simulation of free surface hydrodynamic flows and successfully simulated numerous free surface flow problems such as wave overtopping (Shao *et al.*, 2006), wave-structure interaction (Gotoh *et al.*, 2004; Shao and Gotoh, 2004) and wave breaking (Shao, 2006).

While the ISPH formulations enforce the incompressibility of flow and preserve the linear momentum, they do not generally preserve angular momentum. The angular momentum conservation properties of a SPH formulation strongly influence its performance especially when the model is applied in the

simulation of violent free surface flows (such as the wave breaking and post-breaking) where considerable rigid body motions and rotations with relatively large fluid velocity take place. Bonet and Lok (1999) set forth a discrete variational SPH formulation which ensures the balance of linear and angular momentum. In this paper, analogous to the CSPH formulations proposed in (Bonet and Lok, 1999), new corrective formulations are derived for the ISPH method (Shao and Lo, 2003) to ensure the preservation of angular momentum and thus, to correctly represent the rigid body motions and accurately track the free surface profile. The proposed Corrected ISPH (CISPH) method is applied to the breaking and post-breaking of solitary waves on a plane slope. The high precision of CISPH method, as well as its enhanced performance (compared to ISPH method) in the accurate water-surface tracking and simulation of violent free-surface flows are shown through both quantitative and qualitative comparisons with experimental data.

## 2. Governing Equations

The Lagrangian form of the Navier-Stokes equation is written as follows:

$$\frac{1}{\rho} \frac{D\rho}{Dt} + \nabla \cdot \mathbf{u} = 0 \quad (1)$$

$$\frac{D\mathbf{u}}{Dt} = -\frac{1}{\rho} \nabla P + \frac{1}{\rho} \nabla \cdot \mathbf{T} + \mathbf{g} \quad (2)$$

where  $\rho$  = fluid particle density;  $t$  = time;  $\mathbf{u}$  = particle velocity;  $p$  = particle pressure;  $\mathbf{T}$  = viscous stress tensor; and  $\mathbf{g}$  = gravitational acceleration. It should be noted that Eq. (1) is written in the form of a compressible flow. Incompressibility is enforced by way of setting  $D\rho/Dt = 0$  at each particle in the SPH computation.

## 3. Corrected Incompressible SPH (CISPH), Basics and Formulations

### 3.1 Basic SPH theory

The term “smoothed” in Smoothed Particle Hydrodynamics refers to the procedure for calculating state variables, such as density, in which the function value at a point is determined as a weighted average of values in a local region. In other words, the SPH method is founded on interpolation theory. The conservation laws of continuum dynamics that are in form of Partial Differential Equations (PDE) are

transformed into integral equations through the use of an interpolation function which gives the kernel estimate of the field variables at a point. Computationally, information is known only at discrete points; hence, integrals are evaluated as sums over neighboring particles. For a detailed review of SPH theory, see (Monaghan, 1992). In SPH, the summation interpolant of any function  $A(\mathbf{r})$ , and its gradient are written as:

$$A(\mathbf{r}) = \sum_j m_j \frac{A_j}{\rho_j} W(|\mathbf{r} - \mathbf{r}_j|, h) \quad (3)$$

$$\nabla A(\mathbf{r}) = \sum_j m_j \frac{A_j}{\rho_j} \nabla W(|\mathbf{r} - \mathbf{r}_j|, h) \quad (4)$$

where the subscript  $j$  denotes the physical quantity corresponding to the particle  $j$ ,  $m$  is the mass of particle,  $W$  is an interpolation weighting function and  $h$  is the smoothing length taken as 1.2 times of initial particle spacing in this study. The density of particle  $i$  is obtained by summing over the contributions of the neighboring particles:

$$\rho_i = \sum_j m_j W(|\mathbf{r}_i - \mathbf{r}_j|, h) \quad (5)$$

There are various ways in which the Navier-Stokes equation is represented in SPH (Monaghan, 1992).

The most commonly used form is:

$$\frac{D\rho}{Dt} = \sum_j m_j (\mathbf{u}_i - \mathbf{u}_j) \cdot \nabla_i W_{ij} \quad (6)$$

$$\frac{D\mathbf{u}_i}{Dt} = -\sum_j m_j \left( \frac{P_i}{\rho_i^2} + \frac{P_j}{\rho_j^2} + \Pi_{ij} \right) \nabla_i W_{ij} + \mathbf{g} \quad (7)$$

In the above equations,  $\nabla_i W_{ij}$  = gradient of the kernel with respect to the position of particle  $i$ . The pressure gradient term in the Navier-Stokes equations has a symmetric form and it conserves both linear and angular momentum (as shown in Appendix A).

$$\left( \frac{1}{\rho} \nabla P \right)_i = \sum_j m_j \left( \frac{P_i}{\rho_i^2} + \frac{P_j}{\rho_j^2} \right) \nabla_i W_{ij} \quad (8)$$

The term  $\Pi_{ij}$  is the so-called artificial viscosity which is supposed to represent the effect of viscosity.

The most frequently used artificial viscosity in SPH research is the one proposed by Monaghan (1992):

$$\Pi_{ij} = \begin{cases} \frac{-\alpha \bar{c}_{ij} \mu_{ij} + \beta \mu_{ij}^2}{\bar{\rho}_{ij}} & \mathbf{u}_{ij} \cdot \mathbf{r}_{ij} < 0 \\ 0 & \mathbf{u}_{ij} \cdot \mathbf{r}_{ij} \geq 0 \end{cases} \quad (9)$$

where  $\alpha$  and  $\beta$  are empirical coefficients,  $\bar{c}_{ij} = (c_i + c_j)/2$  is the mean sound speed,  $\bar{\rho}_{ij} = (\rho_i + \rho_j)/2$  and  $\mu_{ij} = (h \mathbf{u}_{ij} \cdot \mathbf{r}_{ij}) / (\mathbf{r}_{ij}^2 + 0.01h^2)$ , with  $\mathbf{u}_{ij} = \mathbf{u}_i - \mathbf{u}_j$  and  $\mathbf{r}_{ij} = \mathbf{r}_i - \mathbf{r}_j$ . There are few advantages and disadvantages associated with the artificial viscosity term. In addition to being a Galilean invariant, such kind of viscosity term conserves both linear and angular momentum and vanishes for rigid body rotations (Monaghan, 1992). However, it is a scalar viscosity which cannot take the flow directionality into account. In addition, it leads to strong dissipation in some cases of flow simulation (Dalrymple and Rogers, 2005) like the case of complex shearing flows where a too large vorticity decay and unphysical momentum transfer are present (Ellero *et al.*, 2002). Hence, it is preferable to model the viscosity in a realistic manner, while, preserving the advantages of the artificial viscosity term.

A few expressions for treatment of realistic viscosity in the SPH calculations exist, among which are the realistic viscosity expressions of Watkins *et al.* (1996) and Takeda *et al.* (1994). The former includes nested summations over the particles (which significantly increases the computational effort), while the latter involves second derivatives of the kernel. The disadvantage of employing second order derivatives is the increase in susceptibility of interpolation to error (Morris *et al.*, 1997). Another approach lies in the introduction of a hybrid term that combines a standard SPH first derivative with a finite difference approximation of the first derivative (Morris *et al.*, 1997; Cummins and Rudman, 1999; Lo and Shao, 2002). The only main shortcoming corresponding to this approach is that, although such hybrid expressions exactly preserve linear momentum, they do not guarantee the conservation of angular momentum (as discussed in Appendix A). In this paper, based on the variational approach proposed by Bonet and Lok (1999), corrective terms are developed to locally modify the hybrid viscosity expression (Shao and Lo, 2003), so that it exactly preserves angular momentum.

### 3.2 CISPH: equation solution process

The important feature which makes the ISPH method distinctive from the original SPH and the WCSPH is that in ISPH method the pressure is determined implicitly through solving a Poisson pressure equation rather than an equation of state. This algorithm was originally proposed by Koshizuka and Oka

(1996), who enforced the incompressibility of flow in their MPS-based calculations. In the ISPH method similar to the MPS method, the governing equations are solved through a two-step prediction-correction process as stipulated by Shao and Lo (2003). The first prediction step is an explicit integration in time without enforcing incompressibility, while, the second correction step is an implicit computation of a divergence free velocity field. In the first process, intermediate temporal particle velocities and positions are obtained without considering the pressure term. In this process the mass conservation or the incompressibility of fluid is not satisfied, in other words, instantaneous particle densities deviate from the initial density. Hence, a second corrective process is required to adjust fluid densities at the particles to the initial constant values prior to the time step. In the correction process, the pressure term is used to update the particle intermediate velocities. The pressure is implicitly calculated from a Poisson pressure equation formulated by combining the mass and momentum equations (1) and (2). The semi-implicit approach employed in MPS, ISPH and CISP methods is very similar to that utilized in a typical grid method (Chorin, 1967).

### 3.3 CISP: formulations

From equation (4), the velocity divergence of particle  $i$  can be formulated as:

$$\nabla \cdot \mathbf{u}_i = \sum_j \frac{m_j}{\rho_j} \mathbf{u}_j \cdot \nabla_i W_{ij} \quad (10)$$

However, higher accuracy will be obtained if the above equation is rewritten with the density placed inside operators (Monaghan, 1992):

$$\nabla \cdot \mathbf{u} = [\nabla \cdot (\rho \mathbf{u}) - \mathbf{u} \cdot \nabla \rho] / \rho \quad (11)$$

Thus:

$$\nabla \cdot \mathbf{u}_i = \sum_j \frac{m_j}{\rho_j} (\mathbf{u}_j - \mathbf{u}_i) \cdot \nabla_i W_{ij} = \sum_j \frac{m_j}{\rho_j} (\mathbf{u}_{ji}) \cdot \nabla_i W_{ij} \quad (12)$$

where  $\mathbf{u}_{j,i}$  is the relative velocity of neighboring particles  $j$  with respect to particle  $i$ . In a similar manner:

$$\left( \frac{1}{\rho} \nabla \cdot \mathbf{T} \right) = \nabla \cdot \left( \frac{\mathbf{T}}{\rho} \right) + \frac{\mathbf{T}}{\rho^2} \nabla \rho \quad (13)$$

Therefore, the viscous stress term in the Navier-Stokes equation can be formulated as:

$$\left( \frac{1}{\rho} \nabla \cdot \mathbf{T} \right)_i = \sum_j m_j \left( \frac{\mathbf{T}_i}{\rho_i^2} + \frac{\mathbf{T}_j}{\rho_j^2} \right) \cdot \nabla_i W_{ij} \quad (14)$$

Since in case of the free surface simulations, large variations in particle density exist near the free surface, the particle densities are replaced by the arithmetic average of particle densities of particle  $i$  and  $j$ , i.e.:

$$\rho_i \rightarrow (\rho_i + \rho_j)/2 \quad ; \quad \rho_j \rightarrow (\rho_i + \rho_j)/2 \quad (15)$$

Hence:

$$\left( \frac{1}{\rho} \nabla \cdot \mathbf{T} \right)_i = \sum_j m_j \left( \frac{4(\mathbf{T}_i + \mathbf{T}_j)}{(\rho_i + \rho_j)^2} \right) \cdot \nabla_i W_{ij} \quad (16)$$

By relating the stress tensor to the rate of strain of flow, the strain-based viscosity would be:

$$\left( \frac{1}{\rho} \nabla \cdot \mathbf{T} \right)_i = \sum_j m_j \frac{(8\nu_0)}{(\rho_i + \rho_j)^2} (\rho_i \mathbf{S}_i + \rho_j \mathbf{S}_j) \cdot \nabla_i W_{ij} = \sum_j m_j \frac{(8\nu_0 \rho_j)}{(\rho_i + \rho_j)^2} (\mathbf{S}_{ji}) \cdot \nabla_i W_{ij} \quad (17)$$

where  $\nu_0$  = the laminar kinematic viscosity and  $\mathbf{S}$  = strain rate tensor. In two dimensions, the rate of strain for neighboring particles  $j$  with respect to particle  $i$  can be written as:

$$\mathbf{S}_{ji} = \begin{bmatrix} \left( \frac{\partial u_x}{\partial x} \right)_{ji} & \left( \frac{1}{2} \left[ \frac{\partial u_x}{\partial y} + \frac{\partial u_y}{\partial x} \right] \right)_{ji} \\ \left( \frac{1}{2} \left[ \frac{\partial u_x}{\partial y} + \frac{\partial u_y}{\partial x} \right] \right)_{ji} & \left( \frac{\partial u_y}{\partial y} \right)_{ji} \end{bmatrix} \quad (18)$$

Employing the chain rule of differentiation and applying the finite difference approximations of the first derivative, the velocity gradients for each particle can be obtained as:

$$\left( \frac{\partial u_x}{\partial x} \right)_{ji} = \left( \frac{\partial u_x}{\partial r} \frac{\partial r}{\partial x} \right)_{ji} = \frac{u_{x_{ji}}}{r_{ij}} \frac{x_{ji}}{r_{ij}} = \frac{u_{x_{ij}}}{r_{ij}} \frac{x_{ij}}{r_{ij}} \quad (19)$$

in which

$$u_{x_{ji}} = u_{x_j} - u_{x_i} \quad ; \quad u_{x_{ij}} = u_{x_i} - u_{x_j} \quad (20)$$

$$x_{ji} = x_j - x_i \quad ; \quad x_{ij} = x_i - x_j \quad (21)$$

$$r_{ij} = |\mathbf{r}_{ij}| = |\mathbf{r}_i - \mathbf{r}_j| \quad (22)$$

By defining a non-dimensional parameter as the relative distance between two particles,  $Q = |\mathbf{r}|/h$ , the

total derivative of the kernel would be:

$$\nabla_i W_{ij} = \frac{\partial W_{ij}}{\partial x} \mathbf{i} + \frac{\partial W_{ij}}{\partial y} \mathbf{j} = \frac{\partial W_{ij}}{\partial Q} \frac{1}{h} \frac{x_{ij}}{r_{ij}} \mathbf{i} + \frac{\partial W_{ij}}{\partial Q} \frac{1}{h} \frac{y_{ij}}{r_{ij}} \mathbf{j} \quad (23)$$

in which:

$$y_{ij} = y_i - y_j \quad (24)$$

Therefore, the SPH formulation of viscosity simplifies to:

$$\left( \frac{1}{\rho} \nabla \cdot \mathbf{T} \right)_i = \sum_j \frac{m_j}{(\rho_i + \rho_j)^2} \frac{4\nu_0 \rho_j}{r_{ij}^2} \begin{bmatrix} 2u_{x_{ij}} x_{ij} \mathbf{i} & (u_{y_{ij}} x_{ij} + u_{x_{ij}} y_{ij}) \mathbf{j} \\ (u_{y_{ij}} x_{ij} + u_{x_{ij}} y_{ij}) \mathbf{i} & 2u_{y_{ij}} y_{ij} \mathbf{j} \end{bmatrix} \cdot \begin{bmatrix} \frac{\partial W_{ij}}{\partial Q} \frac{x_{ij}}{r_{ij} h} \mathbf{i} \\ \frac{\partial W_{ij}}{\partial Q} \frac{y_{ij}}{r_{ij} h} \mathbf{j} \end{bmatrix} \quad (25)$$

The above formulation is the one applied in ISPH method of Shao (2006). In CISP, this formulation of viscosity is modified so that it conserves angular momentum exactly. The modification of the viscosity term is performed by applying some corrective terms which will be discussed in 3.4.

In ISPH and CISP, the Laplacian for pressure is formulated in a similar way to the formulation of viscosity, i.e. as a hybrid of a standard SPH first derivative with a finite difference approximation for the first derivative, and represented also in a symmetrical form by applying the arithmetic averaging for particle densities (Shao, 2006):

$$\nabla \cdot \left( \frac{1}{\rho} \nabla P \right)_i = \sum_j m_j \frac{8}{(\rho_i + \rho_j)^2} \frac{P_j \mathbf{r}_{ij} \cdot \nabla_i W_{ij}}{|\mathbf{r}_{ij}|^2} \quad (26)$$

The formulation of pressure gradient in both ISPH and CISP methods is the same as that of the original SPH, i.e. equation (8).

### 3.4 CISP: corrective terms

In the absence of external forces, the motion of a continuum or particles representing a continuum must be such that the total linear and angular momentum is preserved. In the ISPH model, although the pressure gradient term (equation 8) preserves both linear and angular momentum, the hybrid viscosity expression does not conserve the angular momentum. Preservation of angular momentum can be guaranteed by enforcing the invariance of potential energy with respect to the rigid body motions, as demonstrated by Bonet and Lok (1999). For a general three-dimensional domain by considering an angular velocity vector,  $[w_x, w_y, w_z]^T$ , the velocity vector at any given point can be written as:

$$\mathbf{u}(\mathbf{r}) = \mathbf{w} \times \mathbf{r} \quad (27)$$

The true gradient of this velocity field can be found by:

$$\nabla \mathbf{u} = \mathbf{W}; \quad \mathbf{W} = \begin{bmatrix} 0 & -w_z & w_y \\ w_z & 0 & -w_x \\ -w_y & w_x & 0 \end{bmatrix} \quad (28)$$

Considering the skew nature of  $\mathbf{W}$ , the rate of deformation tensor  $\mathbf{d} = (\nabla \mathbf{u} + \nabla \mathbf{u}^T)/2$  and its trace  $\text{div} \mathbf{u}$  obviously vanish. Consequently, in the absence of approximations resulted by the discretization, the total potential energy would be independent of rigid body translations. Meanwhile, in the SPH method the velocity gradient has the following form:

$$\nabla \mathbf{u}_i = \sum_j V_j (\mathbf{u}_j - \mathbf{u}_i) \otimes \nabla_i W_{ij} \quad (29)$$

$$\nabla \mathbf{u}_i = \sum_j V_j (\mathbf{W} \mathbf{r}_j - \mathbf{W} \mathbf{r}_i) \otimes \nabla_i W_{ij} = \mathbf{w} \sum_j V_j (\mathbf{r}_j - \mathbf{r}_i) \otimes \nabla_i W_{ij} \quad (30)$$

in which  $V_j$  is the volume associated with particle  $j$ . Therefore, the correct skew tensor would be obtained only if the following matrix condition is satisfied by the gradient of kernel function (Bonet and Lok, 1999).

$$\sum_j V_j (\mathbf{r}_j - \mathbf{r}_i) \otimes \nabla_i W_{ij} = \mathbf{I} \quad (31)$$

As an alternative to ensure that equation (31) is satisfied, kernel gradients can be modified by applying a corrective matrix  $L$ :

$$\tilde{\nabla}_i W_{ij} = L_i \nabla_i W_{ij} \quad (32)$$

The velocity gradient is therefore computed as:

$$\nabla \mathbf{u}_i = \sum_j V_j (\mathbf{u}_j - \mathbf{u}_i) \otimes \tilde{\nabla}_i W_{ij} = \sum_j V_j (\mathbf{u}_j - \mathbf{u}_i) \otimes L_i \nabla_i W_{ij} \quad (33)$$

The correction matrix  $L$  is obtained at each particle by enforcing that equation (31) is satisfied by the corrected gradient:

$$\sum_j V_j (\mathbf{r}_j - \mathbf{r}_i) \otimes \tilde{\nabla}_i W_{ij} = \left( \sum_j V_j (\mathbf{r}_j - \mathbf{r}_i) \otimes \nabla_i W_{ij} \right) L_i^T = \mathbf{I} \quad (34)$$

Thus:

$$L_i = \left( \sum_j V_j \nabla_i W_{ij} \otimes (\mathbf{r}_j - \mathbf{r}_i) \right)^{-1} \quad (35)$$

The employment of this correction guarantees that the gradient of any linear velocity field is exactly evaluated. Moreover, angular momentum will be preserved since the internal forces are derived from a variational principle. In view of the fact that the pressure gradient terms in the ISPH calculations preserve

both linear and angular momentum, the above corrective term is only applied during the calculation of viscous accelerations. By enforcing the preservation of angular momentum for viscous internal forces, the new CISP method exactly preserves both linear and angular momentum.

In two dimensions the corrective matrix for particle  $i$  would have the following form:

$$L_i = \left( \begin{bmatrix} \sum_j V_j \frac{DW_{ij}}{DQ} \frac{x_{ij}}{r_{ij}h} x_{ji} & \sum_j V_j \frac{DW_{ij}}{DQ} \frac{x_{ij}}{r_{ij}h} y_{ji} \\ \sum_j V_j \frac{DW_{ij}}{DQ} \frac{y_{ij}}{r_{ij}h} x_{ji} & \sum_j V_j \frac{DW_{ij}}{DQ} \frac{y_{ij}}{r_{ij}h} y_{ji} \end{bmatrix} \right)^{-1} = \left( \begin{bmatrix} \sum_j -V_j \frac{DW_{ij}}{DQ} \frac{x_{ij}^2}{r_{ij}h} & \sum_j -V_j \frac{DW_{ij}}{DQ} \frac{x_{ij}y_{ij}}{r_{ij}h} \\ \sum_j -V_j \frac{DW_{ij}}{DQ} \frac{x_{ij}y_{ij}}{r_{ij}h} & \sum_j -V_j \frac{DW_{ij}}{DQ} \frac{y_{ij}^2}{r_{ij}h} \end{bmatrix} \right)^{-1} \quad (36)$$

By defining the following terms:

$$AMAT = \frac{\sum_j -V_j \frac{DW_{ij}}{DQ} \frac{x_{ij}^2}{r_{ij}h}}{\left[ \sum_j V_j \frac{DW_{ij}}{DQ} \frac{x_{ij}^2}{r_{ij}h} \sum_j V_j \frac{DW_{ij}}{DQ} \frac{y_{ij}^2}{r_{ij}h} - \left( \sum_j V_j \frac{DW_{ij}}{DQ} \frac{x_{ij}y_{ij}}{r_{ij}h} \right)^2 \right]} \quad (37)$$

$$BMAT = \frac{\sum_j -V_j \frac{DW_{ij}}{DQ} \frac{x_{ij}y_{ij}}{r_{ij}h}}{\left[ \sum_j V_j \frac{DW_{ij}}{DQ} \frac{x_{ij}^2}{r_{ij}h} \sum_j V_j \frac{DW_{ij}}{DQ} \frac{y_{ij}^2}{r_{ij}h} - \left( \sum_j V_j \frac{DW_{ij}}{DQ} \frac{x_{ij}y_{ij}}{r_{ij}h} \right)^2 \right]} \quad (38)$$

$$DMAT = \frac{\sum_j -V_j \frac{DW_{ij}}{DQ} \frac{y_{ij}^2}{r_{ij}h}}{\left[ \sum_j V_j \frac{DW_{ij}}{DQ} \frac{x_{ij}^2}{r_{ij}h} \sum_j V_j \frac{DW_{ij}}{DQ} \frac{y_{ij}^2}{r_{ij}h} - \left( \sum_j V_j \frac{DW_{ij}}{DQ} \frac{x_{ij}y_{ij}}{r_{ij}h} \right)^2 \right]} \quad (39)$$

Therefore, the kernel gradient matrix in equation (25) is replaced by the following corrected kernel gradient matrix:

$$\tilde{\nabla}_i W_{ij} = L_i \nabla_i W_{ij} = \begin{bmatrix} DMAT \frac{\partial W_{ij}}{\partial Q} \frac{x_{ij}}{r_{ij}h} \mathbf{i} - BMAT \frac{\partial W_{ij}}{\partial Q} \frac{y_{ij}}{r_{ij}h} \mathbf{j} \\ -BMAT \frac{\partial W_{ij}}{\partial Q} \frac{x_{ij}}{r_{ij}h} \mathbf{i} + AMAT \frac{\partial W_{ij}}{\partial Q} \frac{y_{ij}}{r_{ij}h} \mathbf{j} \end{bmatrix} \quad (40)$$

### 3.5 CISP: treatment of boundary conditions and free surfaces

The treatment of boundary conditions and free surfaces in the CISP is similar to that in the ISPH method, which has already been discussed in details by Gotoh *et al.* (2004) and Shao and Gotoh (2005). A brief summary is given as follows.

Fixed solid boundaries are treated by fixed wall particles, which balance the pressure of inner fluid particles and prevent them from penetrating the wall. The pressure Poisson equation is also solved on these wall particles analogous to the treatment of wall particles in a grid-based method. In order to impose the homogenous Neumann boundary condition of wall particles, several lines of dummy particles are introduced on the outer side of the wall. The pressure of these dummy particles is set to be equal to the pressure of neighboring wall particles. The incident wave is generated by means of an offshore moving wall, the velocity of which is adjusted according to the analytical solution of solitary waves with desired heights. The free surface can be easily and accurately tracked since the particle density on the free surface drops abruptly due to lack of particles in the outer region of the free surface. The following criterion is considered for the detection of free surface particles:

$$\langle \rho^* \rangle_i < 0.99\rho_0 \quad (41)$$

in which  $\rho^*$  and  $\rho_0$  are the intermediate and initial particle density, respectively.

### 3.6 CISPH: interpolation kernel

The interpolation kernel applied in CISPH is the same kernel applied in the ISPH, namely the cubic B-Spline kernel proposed by Monaghan (1992).

$$\left\{ \begin{array}{ll} W(r, h) = \frac{10}{7\pi h^2} \left(1 - \frac{3}{2}Q^2 + \frac{3}{4}Q^3\right) & Q < 1 \\ W(r, h) = \frac{10}{28\pi h^2} (2 - Q)^3 & 1 \leq Q \leq 2 \\ W(r, h) = 0 & Q > 2 \end{array} \right. \quad (42)$$

This kernel has a compact support, its second derivative is continuous, and the dominant error term in the integral interpolant is  $O(h^2)$  (Monaghan, 1992). Other kernels such as higher-order Spline [e.g. Quintic-Spline (e.g. Morris *et al.*, 1997)], the modified Gaussian (e.g. Colagrossi and Landrini, 2003) or Quadratic kernels (e.g. Dalrymple and Rogers, 2005) have been used in the SPH research.

### 3.7 CISPH: determination of calculation time-step

In the CISPH, the time increment of calculation is set according to Courant stability condition and a time resolution chosen as  $5.0 \times 10^{-4}$  seconds:

$$\Delta t = \min(\alpha_{dt} d_0 / u_{\max}, 5.0 \times 10^{-4}) \quad (43)$$

in which  $\alpha_{dt}$  = ratio of the time step to Courant number (=0.1),  $u_{\max}$  = instantaneous maximum velocity of particles;  $d_0$  = particle diameter or the particle spacing.

#### 4. Numerical simulations of solitary wave breaking and post-breaking on a slope

As highly non-linear physical processes, the wave breaking and post-breaking are of significant engineering importance. However, the complexities of fluid motions associated with such processes bring about many mathematical difficulties which eliminate the chance of a fully theoretical description. Experimental techniques and grid-based numerical methods suffer from certain limitations and difficulties when they are employed in the study of such violent free surface flows (see Gotoh *et al.*, 2005 or Shao, 2006 for more details). On the other hand, particle methods (such as the SPH method) have the potential to provide a comprehensive description of the full processes associated with wave breaking, whilst, they can accurately track the water surface profile during such processes.

In this section, the developed CISPH method is applied to the simulation of solitary wave breaking and post-breaking on a uniform slope. At first, the performance of the present model in the simulation of different types of wave breaking is demonstrated. Afterwards, the capability of the CISPH in the simulation of plunging breaking waves and the resulting post-breaking processes such as the complex process of splash-up is shown through the qualitative comparisons with still photographs taken during the laboratory experiments (Li, 2000; Li and Raichlen, 2003). Followed by the qualitative comparison, the high accuracy of the developed model is verified through the quantitative comparisons of both the CISPH and the ISPH simulation results with those obtained from the laboratory experiment of Li (2000), also those from the VOF and the BEM models.

##### 4.1 Different types of wave breaking on a uniform slope

The forms of the wave at breaking, or the breaking types are classified by the so-called self similarity parameter (Battjes, 1974), which is a function of the slope,  $s$ , the deep-water wave height,  $H_0$ , and the deep-water wavelength,  $L_0$ . Since the wave length and wave period of a solitary wave are theoretically infinite, various approaches have been utilized to define a surf similarity-type parameter for solitary waves, by use of which the breaking types and breaking wave characteristics can be computed. By

considering a horizontal length scale for  $L_0$ , Grilli *et al.* (1997) introduced the following dimensionless slope parameter for solitary waves:

$$S_0 = \frac{sL_0}{h_0} = 1.521 \frac{s}{\sqrt{H'_0}} \quad (44)$$

in which,  $h_0$  is the offshore water-depth and  $H'_0 = H_0/h_0$  is the dimensionless incident solitary wave height.

The above parameter can be used to determine whether or not a solitary wave breaks on a given slope and what type of breaking occurs. Solitary breaking type criteria defined in terms of  $S_0$  are introduced by:

(i)  $0.3 < S_0 < 0.37$  then surging breaking; (ii)  $0.025 < S_0 < 0.3$  then plunging breaking and (iii)  $S_0 < 0.025$  then spilling breaking (Grilli *et al.*, 1997).

A total number of five cases of solitary wave breaking are simulated in the present study. Among which are three cases of plunging breaking and one case of surging and one case of spilling breaking. The simulation conditions of the plunging breaking cases correspond to those of the experimental study of Li (2000). In addition to the developed CISP model, the ISPH model of Shao and Lo (2003) is also applied in the simulation of the plunging breaking cases. The physical conditions of all the five cases and the resulting breaking type are summarized in **Table 1**.

A schematic view of the computation domain for the first three plunging breaking cases (Cases II, III and IV) is depicted in **Fig. 1**. The initial constant water depth in all three cases is 0.200 m. The particles are 0.005 m in diameter and about 20000 particles are employed in the domain. Since the waves are generated by a moving wall (which initially moves backward) and a constant number of particles are employed, by the time when the desired wave is generated, the offshore water depth is less than that of the initial one. In order to achieve the desired relative wave heights, the corresponding solitary wave heights are obtained based on a process of trial and error and through numerous simulations.

The profile of a solitary wave as a function of distance  $x$  and time  $t$  is defined as:

$$\eta(x,t) = H_0 \operatorname{sech}^2[n(x - Ct)] \quad (45)$$

in which  $C$  is the celerity of the wave and  $n$  is given by:

$$n = \sqrt{\frac{3H_0}{4h_0^3}} \quad (46)$$

**Fig. 2** shows the comparison between the analytical and the simulated wave profile for the simulation case II. It can be seen that the numerical wave profile agrees well with the analytical one.

**Fig. 3** is depicted based on equation (44). The conditions of the five cases of wave breaking are shown on this figure. Typical CISPH snapshots of three types of wave breaking, namely spilling (Case V), plunging (Case III) and surging (Case I) breaking are shown in **Fig. 4**.

Another classification of wave breaking types has been introduced based on the amount and variation of the angular momentum at the wave front (Koshizuka *et al.*, 1998). In plunging breaking waves, angular momentum at the wave front abruptly changes from a small positive value to a relatively larger negative value. Conversely, in the spilling breaking waves, the angular momentum at the wave front slightly varies around 0.0. The value of the minimum angular momentum at the wave front has been considered as a criterion to classify the plunging and spilling breaking waves in the study of Koshizuka *et al.* (1998). The variation of angular momentum at the wave front for the simulation cases II and V is depicted in **Fig. 5(a)** and **(b)**, respectively. The definition of angular momentum at the wave front is similar to that in (Koshizuka *et al.*, 1998). Two regions with radius of interaction or  $r_e$  (which is  $2h$  in this study) are considered, one at the top of the wave ( $=A_1$ ) and the other at  $L_0/20$  ahead ( $=A_2$ ). A practical value for the solitary wavelength was used here. In a solitary wave the water surface elevation decays fast with  $x$ ; hence, an arbitrarily wavelength as  $L=2\pi/(nH^{1/2})$  can be considered for practical purposes. At a distance of  $x=L/2$  from the crest, the water surface profile is calculated as  $\eta(x,t) = H_0 \text{sech}^2(\pi/\sqrt{H_0})$  which is nearly zero. A schematic sketch of the definition of angular momentum at the wave front is given in **Fig. 6**. The angular momentum is calculated from the following formula:

$$\omega = \frac{1}{N} \sum_{i \in A_1, A_2} \mathbf{r}_i \times \mathbf{u}_i \quad (47)$$

where  $N$  is the number of particles in the regions  $A_1$  and  $A_2$ . Vectors  $\mathbf{r}_i$  and  $\mathbf{u}_i$  are the positions and the velocities of particles, respectively. The origin of the position vectors is considered to be the center between  $A_1$  and  $A_2$ . The parameter  $\omega_1$  is used for normalizing the y axis in **Fig. 5(a-b)**. This parameter is chosen as:

$$\omega_1 = \frac{L_0}{20} \times \sqrt{gh_0} \quad (48)$$

From **Fig. 5(a-b)** it can be seen that the variation of angular momentum agrees well with the statements of Koshizuka *et al.* (1998). In case of the plunging breaking [**Fig. 5(a)**], a sharp drop can be seen in the quantity of the angular momentum from a relatively small positive value to a relatively large

negative value and then it remains negative until the impact of the plunging jet. On the other hand, in case of the spilling breaking [Fig. 5(b)] the angular momentum slightly varies from a relatively small positive value to a smaller negative value, followed by that it gradually reaches a positive value which is very close to zero. Hence, it can be concluded that the CISP model is capable of simulating different types of wave breaking.

#### 4.2 Qualitative comparison

Fig. 7 depicts some CISP snapshots of plunging breaking for the simulation case III. The conditions of the incident relative wave height of  $H_0/h_0 = 0.40$  together with the slope of 1:15 result in a large-scale plunging breaking in which the plunging jet hits the still water ahead of the wave (and not the dry slope), thus a secondary shoreward directed jet is generated from the impact point. This jet impact initiates the splash-up process. The initiation of the splash-up can be seen at Fig. 7(b). The splash-up is a very complex, yet important process as it is responsible for the generation of large-scale vortices and plays a major role in the dissipation of wave energy and momentum transfer. The complexities of the fluid behaviour such as the existence of large deformations and fragmentations have made the simulation of such a process very difficult. In this section, the capability of the CISP model in the simulation of plunging wave breaking and the resulting splash-up process is demonstrated through the qualitative comparison with laboratory photographs (Li, 2000; Li and Raichlen, 2003).

Fig. 8 illustrates the plunging breaking and the splash-up process of a solitary wave with conditions corresponding to simulation case III. In the middle part of the figure, the still photographs are those taken during laboratory experiments (Li, 2000; Li and Raichlen, 2003), while, the CISP and ISPH results are shown on the right and left hand sides, respectively. The CISP snapshots are qualitatively well compared to the laboratory photographs. The development and impact of the plunging jet, together with the resulting splash-up process are well reproduced. On the other hand, the ISPH model could only moderately simulate the development of the plunging jet, while the highly non-linear splash-up process could not be simulated at all.

The SPH-based models are capable of simulating such non-linear processes when the angular-momentum-preserved artificial viscosity terms are employed (Dalrymple and Rogers, 2005; Colagrossi, 2004). Nevertheless, in case of the ISPH model the highly non-linear processes with

non-linear strain rate of flow are very hard to be simulated because of the employment of a tensor-type realistic viscosity which does not generally preserve angular momentum. In the CISPH model, introduction of correction terms guarantees the preservation of angular momentum and the exact calculation of the gradient of any linear velocity field; thus, the difficulty in the reproduction of complex non-linear processes such as the splash-up process is removed, while, the advantages of ISPH model are maintained.

**Fig. 9(a-c)** is obtained by overlapping the CISPH snapshots on the laboratory photographs. From **Fig. 9(a-b)**, a good coincidence of the CISPH calculations and the photographs can be observed. The accurate CISPH calculations have resulted in precise reproductions of the plunging jet [**Fig. 9(a)**] and the highly fragmented reflected jet [**Fig. 9(b)**]. The presented figure not only underlines the high accuracy of the CISPH model, but demonstrates the potentials of particle methods as superior models for hydrodynamic calculations.

Although the entire stages of plunging breaking and post-breaking are well simulated by the CISPH model, there exist some minor disagreements between the simulation snapshots and the laboratory photographs. The first disagreement lies in the reproduction of the aerated region underneath the plunging jet. Although the void region underneath the plunging jet is quite well simulated at the early stages of splash-up, water particles tend to occupy this void region as the post-breaking proceeds. From **Fig. 8(fc)** it can be seen that the void area underneath the plunging jet is less than that of the laboratory snapshot. A few probable factors might be thought in the explanation of the first disagreement.

Firstly, the CISPH model applied in this study is a single-phase flow model; accordingly, the effect of strong air flow to the region beneath the plunging jet and the resulting entrapped air on water particles is not considered. The evolution of the aerated region beneath the plunging jet could be reproduced as a pure void region by the intrinsically two-phase CIP-based (Yabe *et al.*, 1991; Yabe *et al.*, 2001) models [e.g. Watanabe *et al.* (1998)]. Nevertheless, the single-phase SPH calculations of Colagrossi (2004) could also reproduce such void area during the post-breaking process. Thus, this reason does not seem to be a notable cause of the first disagreement.

The second reason might be that the current CISPH model is the corrected version of the standard ISPH model in which no turbulence model is incorporated. Consequently, the effect of turbulent motions smaller than size of particles is not taken into account and only macroscopic particle-scale behaviour of

water is considered. Lagrangian Sub-Particle-Scale (SPS) turbulence models (Gotoh *et al.* 2001) which are similar to the Sub-Grid-Scale (SGS) turbulence models in grid-based calculations, appear to adjust the particle velocities based on the turbulent state of the flow, and thus, result in more realistic simulation results, especially in case of highly turbulent flows such as the wave breaking. However, since very fine particles are applied in the present study, the effect of the sub-particle-scale turbulent motions does not seem to be significant. Moreover, in the SPH-based calculations of Dalrymple and Rogers (2005) with a SPS turbulence model, the same disagreement seems to be present. Therefore, this reason does not seem to be the main cause of the first disagreement either and as it will be discussed later; the first disagreement is expected to be due to the numerical errors arising from the nature of the SPH interpolations.

The second disagreement between the CISP-H numerical results and the laboratory photographs is seen in the development of the splash-up process and the final reflected jet angle. According to the laboratory photographs, during the development of the splash-up process, the reflected jet curls back toward the incident wave and eventually becomes nearly vertical [**Fig. 8(g)**]; however, in the CISP-H snapshots, the reflected jet appears to stop curling back at the final stages of the splash-up process [**Fig. 8(gc)**]. The existing disagreement is more clearly illustrated in **Fig. 9(c)** where the overlapping of the CISP-H snapshot with its corresponding laboratory photograph is presented. Such disagreement is likely because of the numerical errors in the estimation of the highly non-linear velocity and pressure fields in the reflected jet itself and the area in the vicinity of its toe. The excessive particles that have occupied the area underneath the plunging jet, particularly those near the plunging jet impact point, interfere in the momentum exchange between the plunging jet and the water at the toe of the reflected jet. Such interference results in an artificial shoreward-directed momentum which accelerates the particles at the toe of the reflected jet shoreward, especially at the final stages of splash-up process when more particles are accumulated in the area underneath the plunging jet. The overestimation of the shoreward acceleration of the jet particles itself seems to intensify such disagreement.

The most probable factor behind both the existing disagreements lies in the emergence of numerical errors due to a so-called completeness deficiency of SPH interpolants. This problem was first noticed by Liu *et al.* (1993) and since then has been a major issue in the SPH research [e.g. Johnson and Beissel (1996); Bonet and Kulasegaram (2000); Chen and Beraun (2000)]. In the development of the CISP-H, the

main focus was on the momentum conservation properties of SPH formulations. Nevertheless, in addition to that, for achieving more accurate and realistic velocity and pressure fields, the completeness of SPH interpolants should be guaranteed as well. The completeness in meshfree methods is analogous to the consistency in the finite difference literature, and refers to the ability of the kernel interpolants to exactly reproduce a physical field, based on the nodal (particle) values. Since, the completeness of the SPH interpolants is not precisely guaranteed here, some numerical errors emerge when it comes to the reproduction of highly non-linear velocity fields during the breaking and post-breaking process. By enforcing the high-order completeness or reproducing conditions of SPH interpolants, the highly non-linear velocity fields (and the abrupt irregular strain rates) can be better reproduced and hence, enhanced simulation results might be obtained. Meanwhile, as the main aim of the present study is the accurate tracking of the free surface and since such numerical errors do not appear to considerably affect the water surface profile, in the current version of CISPH the high-order reproducing conditions of the kernel interpolants are not enforced. However, for future work, implementation of such kind of corrections should be considered, especially when the CISPH is supposed to model the details of the highly nonlinear physical processes.

Another interesting issue regarding the CISPH model is the thickness of the free surface boundary. Except for the breaking and post-breaking regions, in other parts of the computational domain, a very thin layer of particles, mainly a one-particle-thick layer is detected as the free surface. Hence, the free surface boundary condition is correctly applied to a very thin free surface boundary layer. **Fig. 10** shows the snapshots of water surface profile for the simulation case IV at 0.1 seconds before breaking. On the upper part the presented snapshot is obtained from the CISPH calculations. In this case the presence of a thin free surface boundary is clear. On the other hand, in case of ISPH, the free surface boundary varies in length across the domain. The thickness of the free surface boundary is about 3 or 4 times larger than that in the CISPH.

#### *4.3 Quantitative comparison*

In order to further evaluate the accuracy of the proposed CISPH model, the simulation results of Cases II and IV are quantitatively compared to their corresponding experimental results (Li, 2000). Comparisons are made in terms of wave breaking characteristics such as variation in wave-height,

geometrical properties of plunging jet and horizontal velocity of the tip of the plunging jet.

**Fig. 11** demonstrates the nearly symmetrical solitary wave shape at the very early stages of shoaling for the simulation case II. The wave shape agrees well with the analytical solution shown by the larger circles on the free surface. From this region shoreward, the wave front becomes continuously steeper until the wave breaks. The breaking point is defined as the point where the front face of the wave crest becomes nearly vertical. The formation of the plunging jet is initiated nearly at the breaking point.

Some snapshots of water particles together with the horizontal velocity field are shown in **Fig. 12** (simulation case IV). On the left hand side, the snapshots are those obtained from the CISP model, while, the ISPH snapshots are demonstrated on the right hand side.

**Fig. 13(a)** shows a comparison of the variation in wave height  $H/H_0$  for the simulation case II, among the BEM (Grilli *et al.*, 1997), coupled VOF/BEM (Lachaume *et al.*, 2003), ISPH and CISP models and experimental data (Li and Raichlen, 1998; Li, 2000). In the figure,  $x_s$  is the location at which the slope starts. As it is evident from the figure, the BEM and coupled VOF/BEM models provide good predictions of wave height in the vicinity of breaking point. However, some overestimations of wave height are seen after the breaking. The BEM model fails to calculate the post-breaking stage as it breaks down in the computation of highly rotational flows. The ISPH prediction of wave height is quite well prior to the impact of the plunging jet. However, near the impact point, an abrupt change is seen in the trend of the wave height variation; hence, the ISPH estimations of wave height come out with considerable errors during the post-breaking stage. The abrupt and large deformations of water accompanied by highly non-linear velocity fields bring about considerable numerical errors in the ISPH post-breaking calculations of a strong or large scale plunging breaking. As a consequence, the water particles become dispersed and an unrealistic wave height is recorded. On the other hand, the exact preservation of angular momentum and more accurate calculation of velocity field allow the CISP to accurately track the water surface all through the stages of breaking and post-breaking. The best prediction of CISP is during the post-breaking stage where it gives the best results among all the numerical models. Before the post-breaking, however, the CISP has slightly underestimated the wave height. This might be because of the excessive dissipation due to the corrective terms.

The variation of wave height  $H/H_0$  for the simulation case IV is plotted in **Fig. 13(b)**, this time as a function of the ratio of the offshore water-depth to the local depth,  $h_0/h_1$ . Similar to the simulation case II,

the ISPH gives good results prior to the impact of the plunging jet. The same false trend in the variation of wave height is observed again in the vicinity of the plunging jet impact. However, this time the amount of relative error is less than that of simulation case II. The CISP models well agree with the experiment and the BEM model, although a little amount of underestimation exists.

Another comparison which can further reveal the accuracy of CISP model in the accurate tracking of the water surface, is the one made in the geometrical properties of the plunging jet. The geometry of the plunging jet was measured in the experimental study of Li (2000) for the same conditions of simulation case IV. Three characteristics were utilized to describe the plunging jet: (i) trajectory of the tip of the plunging jet (ii) the length and thickness of the jet before impingement (iii) the horizontal velocity of the tip of the plunging jet. **Fig. 14** illustrates the CISP and ISPH predictions of the trajectory of the plunging jet tip, while, the experimental data (Li, 2000) are plotted for comparison. On the contrary to the ISPH model, the CISP model has given a very accurate prediction of the motion and location of the plunging jet tip.

The length and thickness of the jet were defined by use of three geometrical parameters. The length of the jet  $L_1$  was defined as the horizontal distance from the tip of the jet to the nearest location of the wave surface which was vertical, as shown in **Fig. 15**. Two other parameters were used to define the thickness of the jet; one is the thickness of the jet at the wave vertical plane ( $=L_2$ ), and the other one ( $=L_3$ ) is the thickness of the jet at half length of the jet or  $L_1/2$ . These three parameters do not only describe the geometrical properties of the jet, but also portray an image of the time and spatial evolution of the wave shape during the development of the plunging jet.

**Fig. 16(a)** depicts the changes in  $L_1$ , the plunging jet length, during its development. Compared to the ISPH, the CISP trend line of plunging jet size is in better agreement to that of the experimental data. Although the size of the jet is underestimated at the breaking point and the early stages of the plunging jet formation, a very good agreement exist between the CISP results and the experimental data during the second-half trajectory of the jet. The variations of  $L_2$  and  $L_3$  are shown in **Fig. 16(b)**. The CISP results closely match with the experimental measurements, in case of  $L_3$ . For the predictions of  $L_2$ ; however, both models have slightly overestimated this length. The ISPH model has also underestimated the length  $L_3$ . It can be seen from the figure that while the lengths  $L_2$  and  $L_3$  remain nearly constant during the development of the jet, the thickness of the jet at the middle ( $=L_3$ ), is about half of that at the base of the

jet ( $=L_2$ ).

The variation of the normalized horizontal velocity of the plunging jet tip is shown in **Fig. 17**. The experimental data are obtained from the high-speed video images by dividing the  $x$  coordinate of the tip in consecutive images by the time interval between frames (Li, 2000). A relatively large variation can be seen in the plotted experimental data, which is thought to be due to the accuracy limitation of the high-speed video (Li, 2000). Nevertheless, the experimental data indicate that the horizontal velocity of the plunging jet tip is nearly constant over most of the jet trajectory, and, as it has been pointed out by other researchers, for example, Skjelbreia (1987), the wave velocity at breaking is of the same order as the wave celerity in constant depth region. The CISPH results agree very well with the experimental data and the wave breaking concepts, while, they do not contain large variations like those seen in the experimental data. According to the CISPH results, at the breaking point, the horizontal velocity of the plunging jet tip is about 85% of the wave celerity. Then, gradually it reaches the wave celerity and remains nearly constant until the impingement of the plunging jet. At the impact point, the horizontal velocity of the plunging jet tip is about 4% higher than the wave celerity. The results obtained from the ISPH, has considerably overestimated the horizontal velocity of the plunging jet tip. The source of discrepancy is expected to be the emergence of numerical errors from the unphysical transport of angular momentum when significant rigid body motions and rotations are about to occur. As a consequence of such unphysical transport, a large number of particles become scattered and attain unrealistic particle accelerations and velocity. On the other hand, the CISPH model is capable of calculating the wave breaking and post-breaking very accurately because of the exact preservation of angular momentum.

## 5. Conclusive Remarks

The paper presents a Corrected Incompressible SPH (CISPH) method for the accurate tracking of the water surface during wave breaking and post-breaking. Based on the variational implications introduced by Bonet and Lok (1999), new corrective terms are derived and employed with the ISPH formulations of Shao and Lo (2003) and Shao (2006). Introduction of corrective terms guarantees the exact calculation of linear velocity fields and ensures the preservation of angular momentum. The CISPH model is applied to the study of breaking and post-breaking of solitary waves on a plane slope. Three different types of wave breaking, namely, spilling, plunging and surging breaking are successfully simulated. The conditions of

breaking types agree well with the breaking criteria of Grilli *et al.* (1997) and the concept of angular momentum variation at the wave front introduced by Koshizuka *et al.* (1998). Qualitative comparisons between both CISP and ISPH results with the laboratory photographs (Li, 2000; Li and Raichlen, 2003) demonstrate the capability of the CISP model in the simulation of plunging breaking waves and the resulting post-breaking processes such as the process of splash-up. The high accuracy of the CISP model is confirmed through quantitative comparisons of CISP results with experimental data and the results obtained from ISPH model and some grid-based numerical models.

The proposed CISP model is a 2D single-phase flow model in which the effect of motions smaller than size of particles or the Sub-Particle-Scale (SPS) turbulence is not taken into account. However, in the present study the main focus was on the angular momentum preservation properties of Incompressible SPH formulations, so that the developed model can accurately reproduce the water surface profile during the breaking and post-breaking of waves on a plane slope. Since the effect of SPS turbulence in the macroscopic behaviour of hydrodynamic flows (such as the water surface profile) does not seem to be significant (Gotoh *et al.* 2005), no SPS turbulence model is incorporated in this study. However, when the CISP model is supposed to simulate a realistic 3D problem, larger computational domain and much more particles are needed. Considering the computational limitations, in such a case large particles with low spatial resolution must be introduced. Therefore, the influence of SPS turbulence becomes significant and turbulence modeling should be considered. Another issue is the parallel computation especially for case of 3D calculations where the computational load will significantly increase. In case of simulation of multi-phase problems such as the wave breaking or surf zone/swash zone sediment transport, introduction of two-phase or multi-phase flows are expected to enhance the simulation results. The key issues for enhanced and practical particle-based calculations of wave breaking are reviewed by Gotoh and Sakai (2006).

In the view point of the particle-based calculations, in addition to the angular momentum preservation aspects, the completeness of interpolants or their ability in exact reproduction of a physical field should be considered. The completeness deficiency of SPH interpolants are expected to result in considerable numerical errors when a highly non-linear process is about to be simulated. Therefore, introduction of other corrective terms for ensuring the completeness of SPH interpolants will help the CISP model to more precisely reproduce the details of the highly non-linear physical processes.

## Appendix A

### *Momentum conservation properties of formulations*

#### *Conservation of linear momentum*

The total linear momentum of a system of particles is given by:

$$\mathbf{G} = \sum_{i=1}^N m_i \mathbf{u}_i \quad (\text{A.1})$$

The motion of each particle is governed by the Newton's second law:

$$\mathbf{F}_i - \mathbf{A}_i = m_i \mathbf{a}_i \quad (\text{A.2})$$

where  $\mathbf{F}$  and  $\mathbf{A}$  denote the external and internal forces acting on particle  $i$  and  $\mathbf{a}$  is the instantaneous particle acceleration. In the absence of external forces, the rate of change of total linear momentum is:

$$\dot{\mathbf{G}} = \sum_{i=1}^N m_i \mathbf{a}_i = -\sum_{i=1}^N \mathbf{A}_i \quad (\text{A.3})$$

Thus the condition for preservation of linear momentum can simply be written as:

$$\sum_{i=1}^N \mathbf{A}_i = 0 \quad (\text{A.4})$$

In general the internal force on particle  $i$  can be expressed as the sum of interaction forces between pairs of particles:

$$\mathbf{A}_i = \sum_{j=1}^M \mathbf{A}_{ij} = 0 \quad (\text{A.5})$$

in which  $M$  is the total number of neighboring particles. A pair of particles, particle  $i$  and its neighboring particle  $j$  is depicted in **Fig. A-1**. It can be shown that both pressure gradient term (equation 8) and viscosity term (equation 25) conserve linear momentum exactly. Writing the kernel gradient as a function of the position vector of particles  $i$  and  $j$ :

$$\nabla_i W_{ij} = \mathbf{r}_{ij} Z_{ij} \quad (\text{A.6})$$

where  $Z_{ij}$  is a scalar function of  $|\mathbf{r}_j - \mathbf{r}_i|$ . Considering the pressure gradient term (equation 8), the force on particle  $i$  owing to  $j$  is then:

$$\mathbf{A}_{j \rightarrow i}^p = m_i m_j \left( \frac{p_i}{\rho_i^2} + \frac{p_j}{\rho_j^2} \right) \mathbf{r}_{ij} Z_{ij} \quad (\text{A.7})$$

Given that  $\nabla_i W_{ij} = \mathbf{r}_{ij} Z_{ij} = -\mathbf{r}_{ji} Z_{ij} = -\nabla_j W_{ij}$ , the above force is exactly equal and opposite to the force on particle  $j$  owing to  $i$ . Consequently, the total sum of all interaction pairs between particles due to pressure gradient will vanish and total linear momentum of the system will be preserved. The same is true for the viscosity term. The  $x$ -direction viscous force on particle  $i$  owing to  $j$  can be written as:

$$A_{j \rightarrow i}^{x-x} = \frac{m_i m_j}{(\rho_i + \rho_j)^2} \frac{4\nu_0 \rho_i}{r_{ij}^2} \left[ 2u_{x_j} x_{ij} \frac{\partial W_{ij}}{\partial x} + (u_{y_j} x_{ij} + u_{x_j} y_{ij}) \frac{\partial W_{ij}}{\partial y} \right] \quad (\text{A.8})$$

which is exactly equal and opposite to the viscous force on particle  $j$  owing to  $i$ . Note that:

$$\nabla_i W_{ij} = \frac{\partial W_{ij}}{\partial x} \mathbf{i} + \frac{\partial W_{ij}}{\partial y} \mathbf{j} = \frac{\partial W_{ij}}{\partial Q} \frac{1}{h} \frac{x_{ij}}{r_{ij}} \mathbf{i} + \frac{\partial W_{ij}}{\partial Q} \frac{1}{h} \frac{y_{ij}}{r_{ij}} \mathbf{j} = - \left( \frac{\partial W_{ij}}{\partial Q} \frac{1}{h} \frac{x_{ji}}{r_{ij}} \mathbf{i} + \frac{\partial W_{ij}}{\partial Q} \frac{1}{h} \frac{y_{ji}}{r_{ij}} \mathbf{j} \right) = -\nabla_j W_{ij} \quad (\text{A.9})$$

and:

$$u_{x_j} x_{ij} = (-u_{x_{ji}})(-x_{ji}) = u_{x_{ji}} x_{ji} \quad (\text{A.10})$$

The same explanation can be given for the  $y$ -direction viscous forces. Therefore, for each pair of particles the viscous interacting forces also vanish. Consequently, the total linear momentum of the system of particles will be exactly conserved in a CISP (or ISPH) calculation.

### *Conservation of angular momentum*

The total angular momentum of the system of particles with respect to the origin is given as:

$$\mathbf{H} = \sum_{i=1}^N \mathbf{r}_i \times m_i \mathbf{u}_i \quad (\text{A.11})$$

By time differentiating and considering the law of motion in the absence of external forces, the rate of change of angular momentum of the system will be:

$$\dot{\mathbf{H}} = \sum_{i=1}^N \mathbf{r}_i \times m_i \mathbf{a}_i = - \sum_{i=1}^N \mathbf{r}_i \times \mathbf{A}_i \quad (\text{A.12})$$

Hence, conservation of angular momentum will be guaranteed if the total moment of the internal forces about the origin vanishes, that is:

$$\sum_{i=1}^N \mathbf{r}_i \times \mathbf{A}_i = 0 \quad (\text{A.13})$$

Considering again the two neighboring particles shown in **Fig. A-1**, the angular moment of the two interacting forces about the origin can be written as:

$$\mathbf{r}_i \times \mathbf{A}_{ij} + \mathbf{r}_j \times \mathbf{A}_{ji} \quad (\text{A.14})$$

If  $\mathbf{A}_{ij} = -\mathbf{A}_{ji}$ , then:

$$\mathbf{r}_i \times \mathbf{A}_{ij} + \mathbf{r}_j \times \mathbf{A}_{ji} = -\mathbf{r}_{ij} \times \mathbf{A}_{ij} \quad (\text{A.15})$$

The above will vanish whenever the interaction force  $\mathbf{A}_{ij}$  is co-linear with the vector  $\mathbf{r}_{ij}$ . Recalling from equation that  $\nabla_i W_{ij}$  is a function of vector  $\mathbf{r}_{ij}$  and a scalar  $Z_{ij}$ , it can be concluded that the angular moment of the two interacting forces between a pair of particles will vanish only if the internal stress tensor is isotropic. In CISP<sub>H</sub> as well as ISP<sub>H</sub> calculations the internal stress tensor is composed of pressure and viscous stresses as follows:

$$\boldsymbol{\sigma} = p\mathbf{I} + \mathbf{T} \quad (\text{A.16})$$

in which  $\mathbf{I}$  is a unit tensor. The first stress tensor, i.e. the internal pressure tensor, is isotropic. Hence, the interacting forces resulting from the internal pressure lie on the same line with the vector  $\mathbf{r}_{ij}$  [Fig. A-2(a)]. As a result, there will be no moment by one pair of interacting pressure forces and the total moment of internal pressure forces will be exactly equal to zero. For the viscous forces, however, this is not the case. Due to the anisotropic nature of the viscous stresses in a realistic viscosity calculation such as in CISP<sub>H</sub> and ISP<sub>H</sub> calculations, the resulting viscous forces do not lie on the same line with the position vector  $\mathbf{r}_{ij}$  [Fig. A-2(b)] and produce a moment. The summation of all the moments between each pair of particles will not necessarily vanish and therefore, angular momentum will not be preserved. In the CISP<sub>H</sub> calculations corrective terms ensure the correct calculation of viscous accelerations and the preservation of angular momentum.

#### References:

- Battjes, J. A., 1974. Surf similarity. Proc., 14th Coast. Eng. Conf., ASCE, 1, pp. 466-480.
- Bonet, J. and Lok, T. S., 1999. Variational and momentum preservation aspects of smooth particle hydrodynamic formulation. Comput. Methods Appl. Mech. Eng. 180, pp. 97-115.
- Bonet, J. and Kulasegaram, S., 2000. Correction and stabilization of smooth particle hydrodynamic methods with applications in metal forming simulations. Int. J. Numer. Methods Eng. 47, pp. 1189-1214.
- Chen, J. K. and Beraun, J. E., 2000. A generalized smoothed particle hydrodynamics method for

- nonlinear dynamic problems. *Comput. Methods Appl. Mech. Eng.* 190, pp. 225-239.
- Chorin, A. J., 1967. A numerical method for solving incompressible viscous flow problems. *Journal of Computational Physics*, 2, pp. 12-26.
- Colagrossi, A. and Landrini, M., 2003. Numerical simulation of interfacial flows by smoothed particle hydrodynamics. *J. Comput. Phys.*, 191, pp. 448-475.
- Colagrossi A., 2004. Dottorato di Ricerca in Meccanica Teorica ed Applicata XVI CICLO, A meshless Lagrangian method for free-surface and interface flows with fragmentation. PhD Thesis, Universita di Roma, La Sapienza.
- Cummins, S. J. and Rudman, M., 1999. An SPH projection method. *J. Comput. Phys.*, 152, pp. 584-607.
- Dalrymple, R.A. and Rogers, B.D., 2005. Numerical modeling of water waves with the SPH method. *Coastal Engineering*, 53, pp. 141-147.
- Ellero, M., Kroger, M. and Hess, S., 2002. Viscoelastic flows studied by smoothed particle dynamics. *Journal of Non-Newtonian Fluid Mechanics*, 105(1), pp. 35-51.
- Gingold, R. A. and Monaghan, J. J., 1977. Smoothed particle hydrodynamics: theory and application to non-spherical stars. *Mon. Not. R. Astron. Soc.*, 181, pp. 375-89.
- Gotoh, H., Ikari, H., Memita, T. and Sakai, T., 2005. Lagrangian particle method for simulation of wave overtopping on a vertical seawall. *Coastal Engineering Journal, JSCE*, 47(2 & 3), pp. 157-181.
- Gotoh, H. and Sakai, T., 2006. Key Issues in the Particle Method for Computation of Wave Breaking. *Coastal Eng.*, 53(2-3), pp. 171-179.
- Gotoh, H., Shao, S. D. and Memita, T., 2004. SPH-LES model for numerical investigation of wave interaction with partially immersed breakwater. *Coastal Eng. Jour., JSCE*, 46(1), pp. 39-63.
- Gotoh, H., Shibahara, T. and Sakai, T., 2001. Sub-Particle-Scale Turbulence Model for the MPS Method -Lagrangian Flow Model for Hydraulic Engineering. *Comput. Fluid Dynamics Jour.*, 9(4), pp. 339-347.
- Grilli, S.T., Svendsen, I.A. and Subramanya, R., 1997. Breaking criterion and characteristics for solitary waves on slopes. *J. Waterway Port Coastal and Ocean Engineering*, 123(3), pp 102-112.
- Johnson, G. R. and Beissel, S. R., 1996. Normalized smoothing functions for SPH impact computations. *Int. J. Numer. Methods Eng.* 39, pp. 2725-2741.
- Koshizuka, S. and Oka, Y., 1996. Moving particle semi-implicit method for fragmentation of incompressible fluid. *Nuclear Science and Engineering*, 123, pp 421-434.

- Koshizuka, S., Nobe, A. and Oka, Y., 1998. Numerical Analysis of Breaking Waves Using the Moving Particle Semi-implicit Method. *Int. J. Numer. Meth. Fluid*, 26, pp. 751-769.
- Lachaume, C., Biauxser, B., Grilli, S. T., Fraunie, P. and Guignard, S., 2003. Modeling of breaking and post-breaking waves on slopes by coupling of BEM and VOF methods. *Proc. 13th Offshore and Polar Engineering Conf., ISOPE03, Honolulu, HI, USA*, pp. 353-359.
- Li, Y. and Raichlen, F., 1998. Breaking criterion and characteristics for solitary waves on slopes-Discussion. *J. Waterways Port Coastal Ocean Engineering*, 124(6), pp. 329-333.
- Li, Y., 2000. Tsunamis: Non-breaking and breaking solitary wave run-up. Rep. KH-R-60, W. M. Keck Laboratory of Hydraulics and Water Resources, California Institute of Technology, Pasadena, CA.
- Li, Y. and Raichlen, F., 2003. Energy balance model for breaking solitary wave runup. *Journal of Waterway, Port, Coastal, and Ocean Engineering*, 129(2), pp. 47-59.
- Libersky, L. and Petschek A. G., 1991. Smooth particle hydrodynamics with strength of materials. *Lecture notes in physics 395: Advances in Free Lagrange Methods*, (Ed. Trease, Fritts and Crowley), Springer-verlag, pp. 248-257.
- Liu, W.K., Adee, J. and Jun, S., 1993. Reproducing kernel and wavelets particle methods for elastic and plastic problems. *Advanced Computational Methods for Material Modeling*, AMD 180/PVP 268 ASME, pp. 175-190.
- Lo, E.Y.M and Shao, S.D., 2002. Simulation of near-shore solitary wave mechanics by an incompressible SPH method. *Applied Ocean Research*, 24, pp. 275-286.
- Lucy, L. B., 1977. A numerical approach to the testing of the fission hypothesis. *Astron. J.*, 82, pp. 1013-24.
- Monaghan, J. J., 1992. Smoothed particle hydrodynamics. *Ann. Rev. Astron. Astrophys.* 30, pp. 543-574.
- Monaghan, J. J., 1994. Simulating free surface flows with SPH. *J. Comput. Phys.* 110, pp. 399-406.
- Monaghan, J. J. and Kocharyan, A., 1995. SPH simulation of multi-phase flow. *Comput. Phys. Commun.*, 87, pp. 225.
- Monaghan, J. J. and Kos, A., 1999. Solitary waves on a Cretan beach. *J. Waterways Port Coastal Ocean Eng.* 125(3), pp. 145-54.
- Monaghan, J. J., Kos, A. and Issa, N., 2004. Fluid motion generated by impact. *J. Waterway Port Coastal Ocean Eng.* 129, 250-259

- Morris J. P., Fox P. J. and Zhu, Y., 1997. Modeling low Reynolds number incompressible flows using SPH. *J. Comput. Phys.* 136, pp. 214-226.
- Muller, M., Schirm, S., Teschner, M., 2004. Interactive Blood Simulation for Virtual Surgery Based on Smoothed Particle Hydrodynamics. *Journal of Technology and Health Care*, 12(1), pp. 25-31.
- Shao, S.D., 2006. Simulation of breaking wave by SPH method coupled with  $k-\varepsilon$  model. *Journal of Hydraulic Research*, 44(3), pp. 338-349.
- Shao, S. D. and Gotoh, H., 2004. Simulation coupled motion of progressive wave and floating curtain wall by SPH-LES model. *Coastal Eng. Jour., JSCE*, 46 (2), pp. 171-202.
- Shao, S. D. and Gotoh, H., 2005. Turbulence particle models for tracking free surfaces. *Journal of Hydraulic Research, IAHR*, 43 (3), pp. 276-289.
- Shao, S. D., Ji, C., Graham, D. I., Reeve, D. E., James, P. W. and Chadwick, A. J., 2006. Simulation of wave overtopping by an incompressible SPH model. *Coastal Engineering*, 53(9), pp. 723-735.
- Shao, S. D. and Lo, E. Y. M., 2003. Incompressible SPH method for simulating Newtonian and non-Newtonian flows with a free surface. *Advanced Water Resources*, 26 (7), pp. 787-800.
- Skjelbreia, J. E., 1987. Observation of breaking waves on sloping bottoms by use of laser Doppler velocimetry. W. M. Keck Laboratory of Hydraulics and Water Resources, California Institute of Technology, Report No. KH-R-48.
- Takeda, H., Miyama, S. M. and Sekiya, M., 1994. Numerical simulation of viscous flow by Smoothed Particle Hydrodynamics. *Prog. Theor. Phys.*, 92(5), pp. 939-960.
- Watanabe, Y., Mori, N. and Saeki, H., 1998. Fluid Motion in a Surf Zone. *Proceedings of 3<sup>rd</sup> International Conference on HydroScience and Engineering*, Brandenburg University of Technology at Cottbus, Cottbus/Berlin, Germany, No. 255.
- Watkins, S. J., Bhattal, A. S., Francis, N., Turner, J. A. and Whitworth, A. P., 1996. A new prescription for viscosity in Smoothed Particle Hydrodynamics. *Astron. Astrophys*, 119, pp. 177-187.
- Yabe, T., Ishikawa, T., Wang, P. Y., Aoki, T., Kadota, Y. and Ikeda, F., 1991. A Universal Solver for Hyperbolic Equations by Cubic-Polynomial Interpolation - II. Two- and Three- Dimensional Solvers, 66, pp. 233-242.
- Yabe, T., Xiao, F., Utsumi, T., 2001. The constrained interpolation profile method for multiphase analysis. *Journal of Computational Physics*, 169, pp. 556-593.

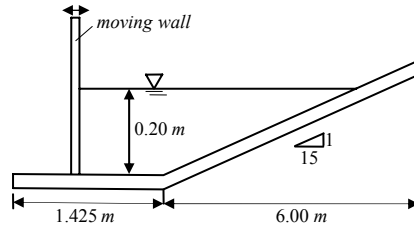


**Fig. 1.** Computational domain for simulation Cases II, III and IV

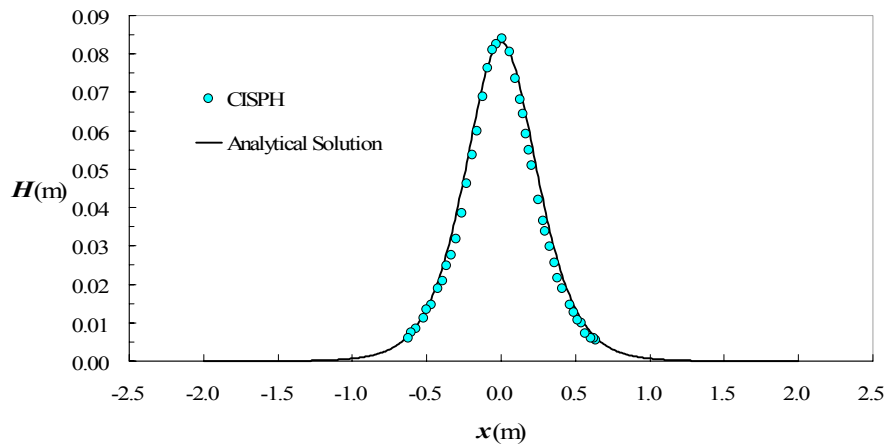


**Fig. 2.** Comparison between the simulated and analytical wave profile – simulation case II

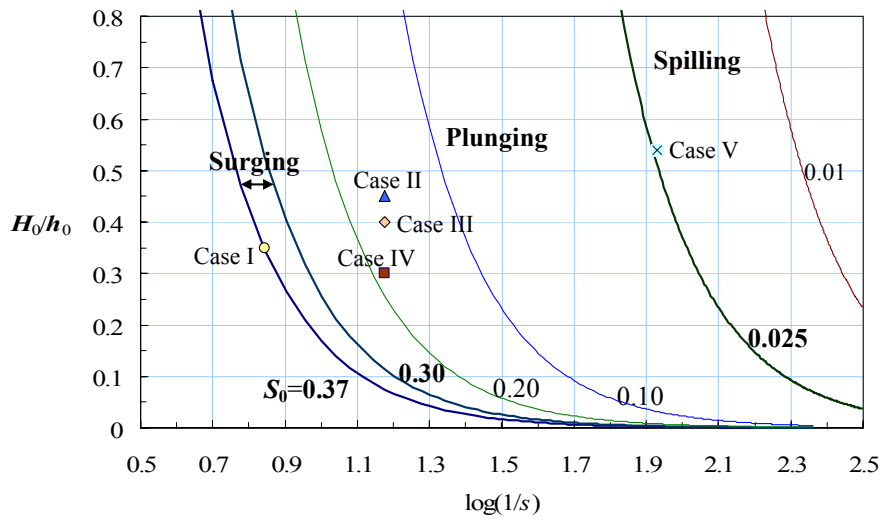


**Fig. 3.** Breaking types and the conditions of the simulation cases

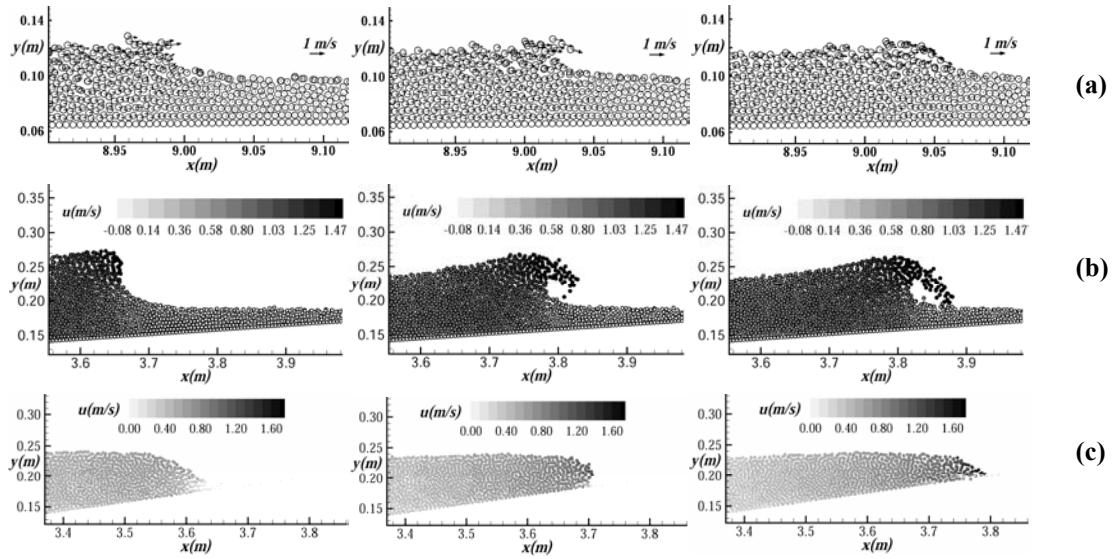


**Fig. 4.** Typical CISPH snapshots of three types of wave breaking, (a) Spilling, (b) Plunging, (c) Surging

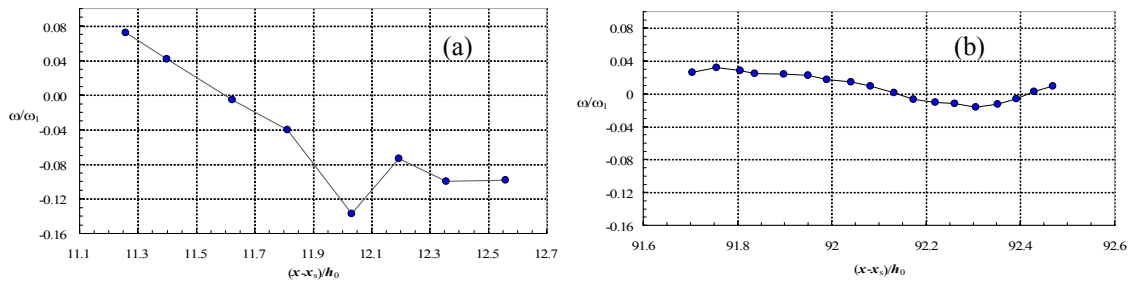


**Fig. 5.** Variation of angular momentum at the wave front (a) in a plunging breaking (simulation case II) - (b) in a spilling breaking (simulation case V)

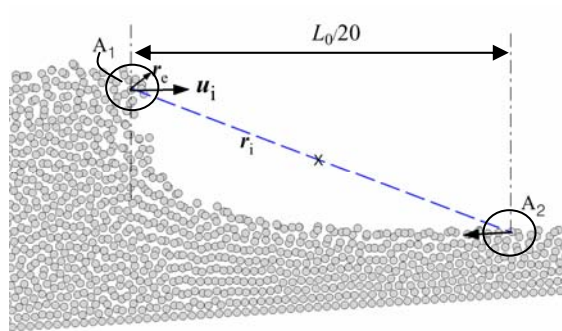


**Fig. 6.** Definition of angular momentum at the wave front

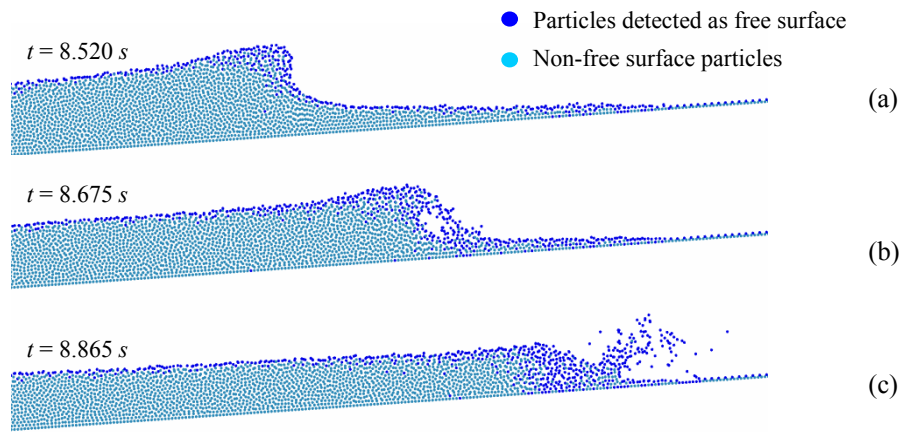


**Fig. 7.** Snapshots of water particles – simulation case III

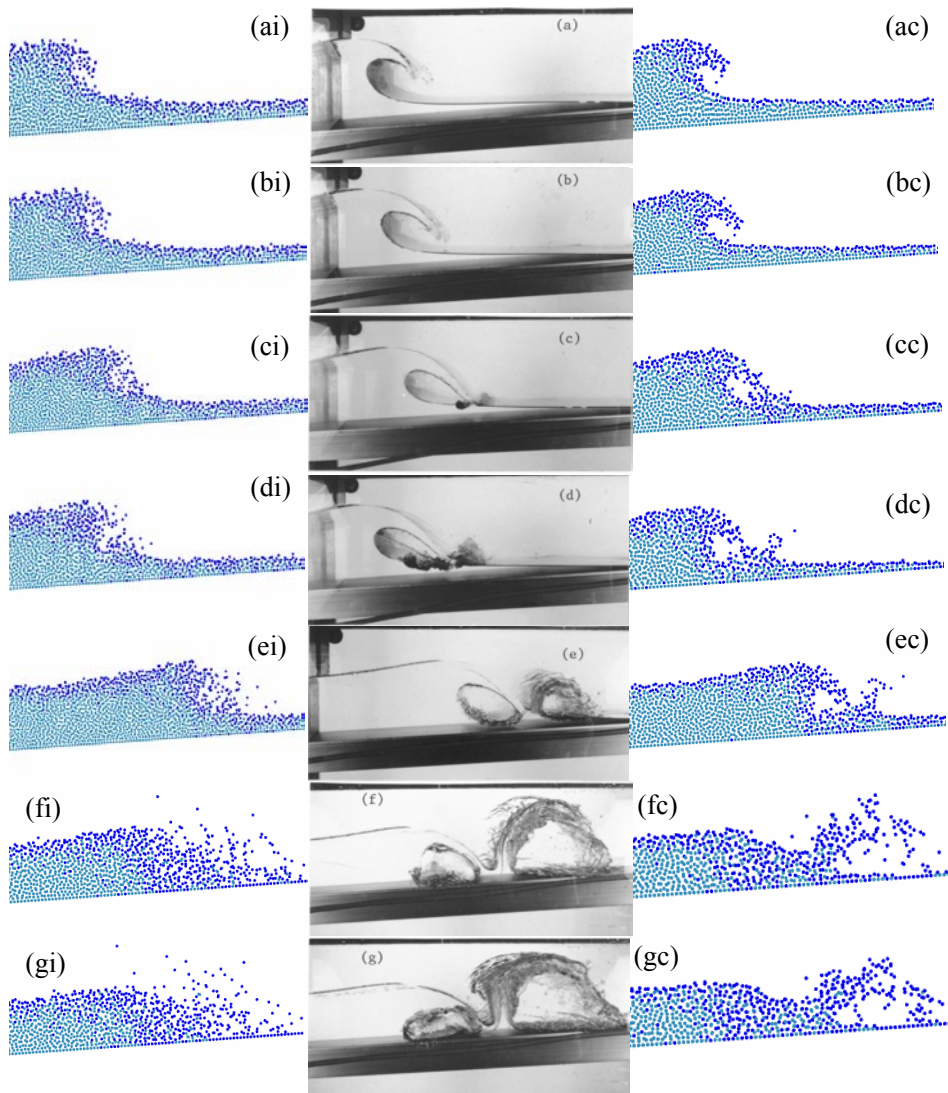


**Fig. 8.** Strong plunging breaking and resulting splash-up – qualitative comparison of laboratory photographs (center) with ISPH (left) and CISP (right) snapshots

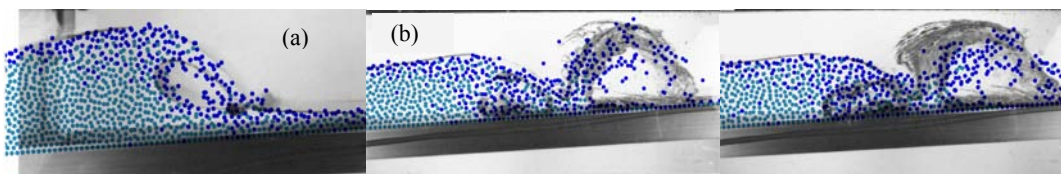


**Fig. 9.** (a) Impact of plunging jet (b) splash-up process (c) final stages of splash-up - overlapping of the CISPH snapshot with laboratory photograph

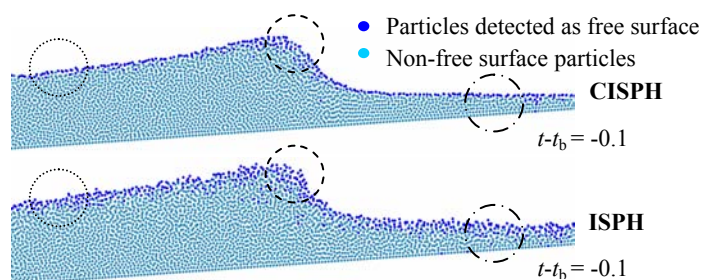


**Fig. 10.** Thickness of free surface boundary in CISPH and ISPH snapshots – simulation case IV

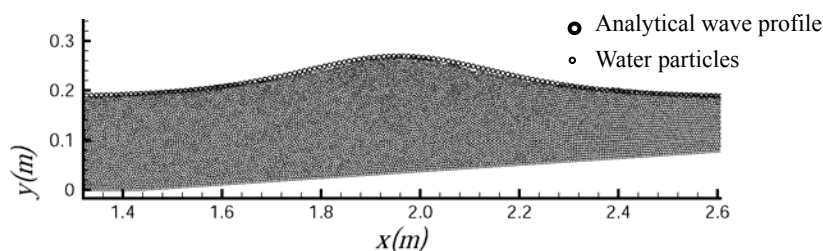


**Fig. 11.** CISPH snapshot of water particles at the very early stages of shoaling – simulation case II

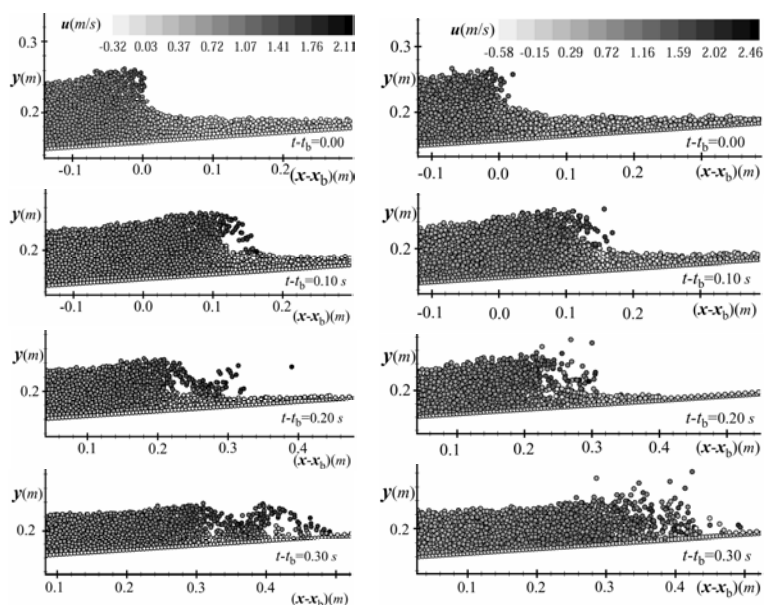


**Fig. 12.** CISPH (left) and ISPH (right) snapshots of water particles and horizontal velocity field – simulation case IV

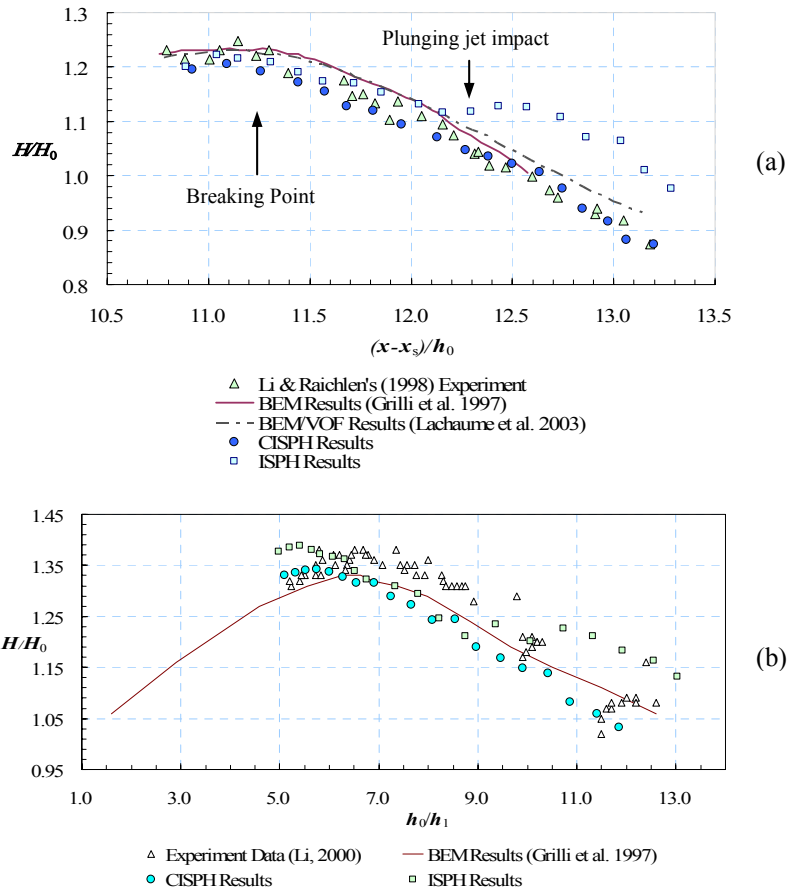


**Fig. 13.** Comparison of variation in wave height during breaking and post-breaking (a) simulation case II  
(b) simulation case IV

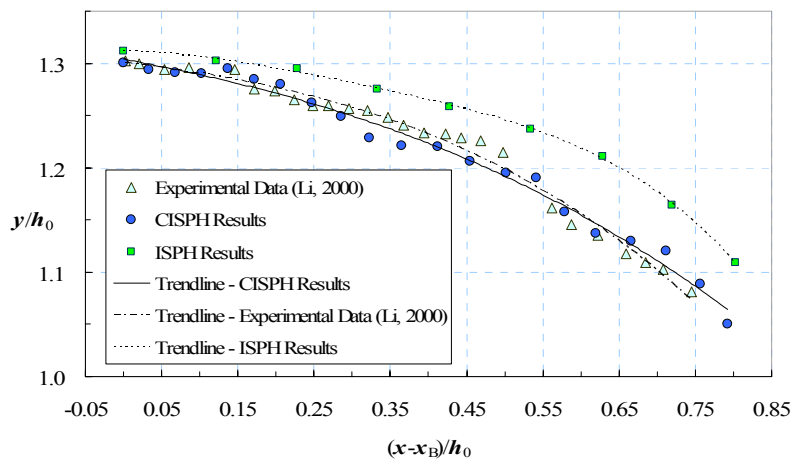


**Fig. 14.** CISPH and ISPH predictions of the trajectory of the plunging jet tip - simulation case IV

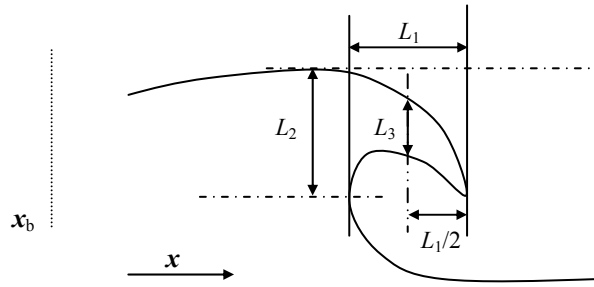


Fig. 15. Definition sketch of the geometrical parameters for describing the plunging jet

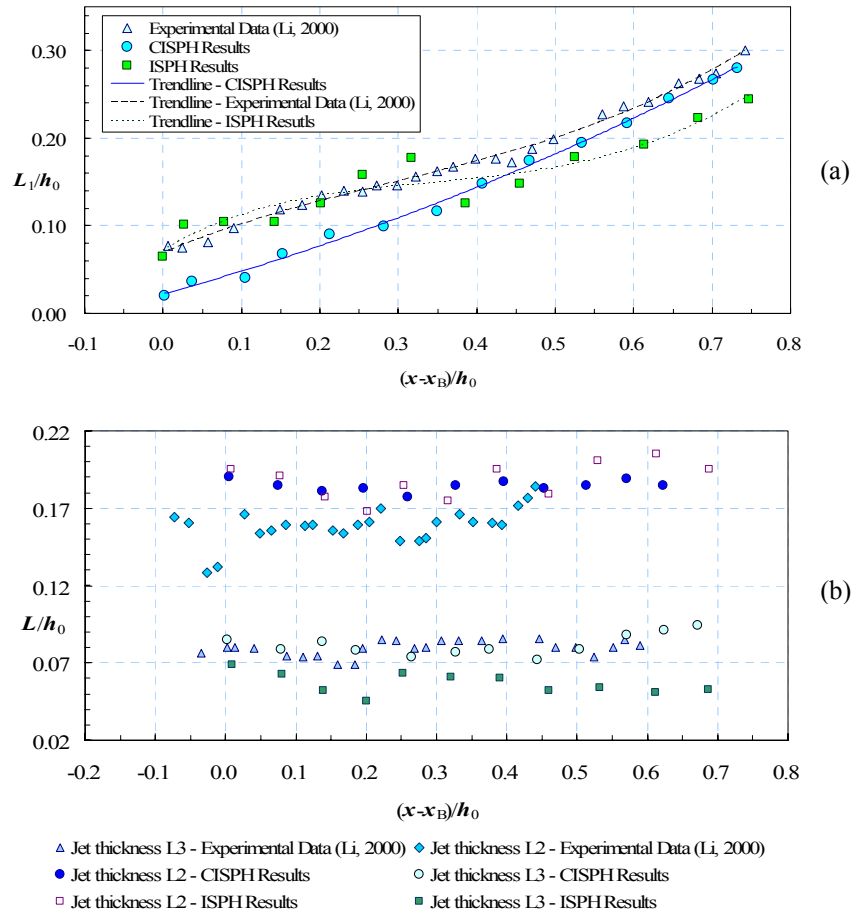
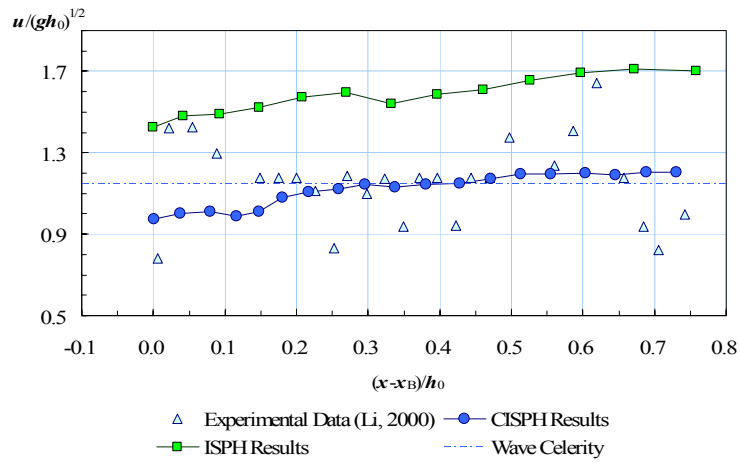
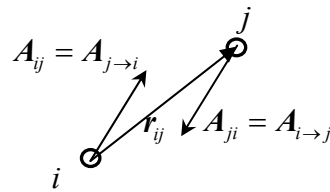


Fig. 16. Comparison between the CISP and ISPH calculations and experimental data (a) Horizontal length ( $L_1$ ) of the plunging jet (b) thicknesses ( $L_2$  and  $L_3$ ) of the plunging jet



**Fig. 17.** Variation of the horizontal velocity of the plunging jet tip - comparison between the CISP and ISPH calculations and experimental data



**Fig. A-1.** Internal interaction forces between two neighboring particles

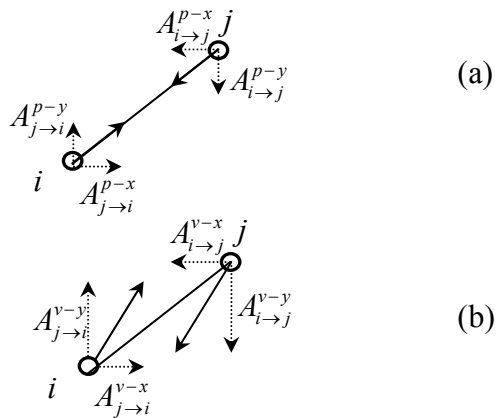


**Fig. A-2.** Decomposition of internal interaction forces between two neighboring particles – (a) internal forces due to pressure (b) internal forces due to viscosity

**Table 1**

Summary of simulation cases – physical conditions and the resulting breaking types

<b>Simulation Case</b>	<b>Wave Height</b>	<b>Offshore Water Depth</b>	<b>Relative Wave Height</b>	<b>Slope</b>	<b><math>S_0</math></b>	<b>Breaking Type</b>
Case I	0.066	0.189	0.35	1:7	0.368	Surging
Case II	0.084	0.186	0.45	1:15	0.152	Plunging
Case III	0.075	0.187	0.40	1:15	0.160	Plunging
Case IV	0.057	0.189	0.30	1:15	0.185	Plunging
Case V	0.053	0.098	0.54	1:85	0.024	Spilling